arXiv:cond-mat/9905278v1 19 May 1999

Infrared and Raman studies of the Verwey transition in magnetite.

L.V. Gasparov and D.B. Tanner

University of Florida, Department of Physics, POBox 118440

Gainesville Fl 32611-8440, USA

D. B. Romero

NIST-Optical Technology Division, Gaithersburg, MD 20899-8441 and Physics Department, University of Maryland, College Park, MD 20742

H.D. Drew

Physics Department, University of Maryland, College Park, MD 20742

H. Berger and G. Margaritondo

Physics Department-IPA, École Polytechnique Fédéral de Lausanne, CH-1015 Lausanne, Switzerland

L. Forró

Physics Department-IGA, École Polytechnique Fédéral de Lausanne, CH-1015 Lausanne, Switzerland

(February 1, 2008)

Abstract

We present infrared and Raman measurements of magnetite (Fe_3O_4). This material is known to undergo a metal-insulator and a structural transition (Verwey transition) at $T_V = 120$ K. At temperatures below T_V, we observe a

strong gap-like suppression of the optical conductivity below 1000 cm^{-1}. The structural aspect of the Verwey transition demonstrates itself by the appearance of additional infrared- and Raman-active phonons. The frequencies of the infrared-active phonons show no significant singularities at the transition whereas their linewidths increase. The frequency and linewidth of the Raman-active phonon at 670 cm^{-1} changes abruptly at the transition. For $T < T_V$, we observe fine structures in the infrared and Raman spectra which may indicate strong anharmonicity of the system below the transition. Our estimate of the effective mass of the carriers above the transition to be $m^* \approx 100m$, where m is the electron mass. Our measurements favor a polaronic mechanism of conductivity and underline the importance of the electron-phonon interaction in the mechanism of the Verwey transition.

71.30.+h, 71.38.+i , 78.30.-j, 78.30.Er, 78.40.-q, 78.40.Kc

Typeset using REVTEX

I. INTRODUCTION

A. The Verwey transition

Charge ordering in strongly-correlated electron systems has recently attracted a lot of attention on account of its possible influence on charge transport and dynamics. In the high-temperature superconductors, there is evidence for the formation of charge and spin stripes near the commensurate doping $x = 1/8$ in $La_{2-x}Sr_xCuO_4$ in which superconductivity is suppressed.[1] The suppression was attributed to the pinning by lattice distortions of the dynamic charge and spin stripes formed in this phase.[2] Very recently Raman scattering in NaV_2O_5 compound revealed considerable charge ordering there at T<35 K.[3] In the manganates, charge ordering is observed at certain commensurate doping.[4] The possibility of the coexistence of ferromagnetic and charge-order correlations may be relevant in understanding the phenomenon of colossal magnetoresistance in manganates. The earliest compound known[5] to manifest charge ordering is magnetite (Fe_3O_4).

Fe_3O_4 is a ferrimagnet below 850 K. At room temperature Fe_3O_4 has an inverse spinel cubic structure with the O_h^7 ($Fd3m$) space group.[6] The unit cell consists of 8 formula units. There are two types of Fe positions in this structure. The so-called A positions are characterized by the tetrahedral oxygen surrounding the Fe ions; the B positions have octahedral oxygen coordination. The A positions are occupied only by Fe^{+3} ions, whereas the B positions are occupied with equal probability by Fe^{+2} and Fe^{+3}.

Magnetite undergoes a first-order transition (the Verwey transition) at $T_V = 120$ K, with changes of crystal structure, latent heat, and a two-order of magnitude decrease of the DC conductivity. This transition was discovered by Verwey[5] in 1939; in his model, the low temperature phase has the Fe^{+2} and Fe^{+3} ions at the B-sites ordered, forming layers of ions of each charge state. Above T_V there is no long-range order, but short-range order persists. According to neutron measurements,[7] an orthorhombic space groups (either a $D_{2h}^{11}, (Pmca)$ or $C_{2v}^2, (Pmc2_1)$) may describe the low temperature structure.

The Verwey transition has been intensively investigated since its discovery, bur remains unexplained. Basically, there are several ideas which partly explain experimental results although none is able to give a complete explanation of the transition. This incomplete theory is probably not surprising in a system where the electron-phonon interaction, the electron-electron interaction, and electronic bandwidth are of nearly the same importance. We shall mention some basic ideas which could lead to an understanding of the transition.

As already mentioned, Verwey and Haayman[8] originally described this transition as an order-disorder transition. The ordered state is insulating, whereas the disordered state is metallic due to the motion of the extra electron on the B-positions. Later, Anderson[9] argued that short range order (SRO) is crucial for understanding the transition. He demonstrated that certain SRO configurations are energetically favorable (Anderson's condition). In this picture, long range order is destroyed above the transition although short-range order, satisfying Anderson's conditions, persists above the transition. The presence of SRO above the transition was confirmed by neutron measurements. However, there is still a question why an abrupt increase in conductivity is observed in spite of the persistence of SRO above the transition.[10]

Cullen and Callen[11] presented a picture of the transition in which only electron-electron correlations are relevant. It is assumed, that an Fe^{+2} ion can be represented as an Fe^{+3} ion plus an extra electron. In this case, the physics of Fe_3O_4 is just the physics of the interaction of this extra electron with a crystal of Fe^{+3} ions. The interaction can be described by the Coulomb nearest neighbor repulsion and hopping integral for the extra electron. The competition between these two values determines whether an insulator or metal is obtained.

In contrast Mott,[10,12] Chakraverty,[13] and Yamada[14] emphasized the importance of the electron-phonon interaction. In the Mott[10] picture of the Verwey transition, the charge carriers are either polarons or bipolarons. Above the transition, the system can be described as a Wigner glass, a system where carriers are localized by the disorder-induced random-field potentials. When the temperature is raised, some of the polarons dissociate leading to a hopping type of conductivity.

One should note however that an activated conductivity could also be accounted for by the opening of a charge gap. Recent photoemission studies[15] of magnetite indicate a charge gap of 150 meV below $T_{\rm V}$. A recent optical measurement on magnetite[16] found that the main temperature-dependent changes of optical conductivity occur below 1 eV, connected with a gap-like temperature-dependant increase of optical conductivity at 140 meV, followed by a broad polaronic peak at 0.6 eV. The gap-like behavior was attributed to the opening of a charge gap. The authors of Ref. 16 suggested that the charge gap, determined as the onset of the polaronic band in the spectra below the transition, is consistent with the gap value found in photoemission studies. In contrast to the statement of Ref. 16, we must note that photoemission measures the transitions to the Fermi level, whereas infrared spectroscopy measures an optically-allowed transition from one electronic band to another across the Fermi level. This means that the optical gap of 140 meV would correspond to smaller gap, perhaps as small as 70 meV, measured in photoemission. Moreover, according to Ref. 15, the gap does not close above transition but rather decreases by only 50 meV, which is not consistent with the analysis of the optical conductivity of Ref. 16.

In this paper we present the results of systematic temperature-dependant infrared and Raman measurements of magnetite and discuss both lattice and charge dynamics, as well as a possible mechanism of Verwey transition.

B. Optical phonons in magnetite

Above the Verwey transition temperature, $T > T_{\rm V} = 120$ K, magnetite has a cubic-inverse-spinel structure belonging to the space group $\mathrm{O}_h^7(Fd3m)$. The full unit cell contains 56 atoms but the smallest Bravais cell contains only 14 atoms. As a result, one should expect 42 vibrational modes. Group theory predicts the following modes for this phase.

$$A_{1g} + E_g + T_{1g} + 3T_{2g} + 2A_{2u} + 2E_u + 5T_{1u} + 2T_{2u}.$$

The T_{1g}, A_{2u}, E_u, and T_{2u} are silent. Thus, there are five Raman-active modes ($A_{1g} + E_g + 3T_{2g}$) and five infrared-active modes ($5T_{1u}$).

When the system undergoes the Verwey transition, the symmetry of the crystal lowers to orthorhombic. The unit cell doubles along the z direction and the diagonals of the former cubic unit cell become the faces of the low-temperature unit cell. As mentioned in Ref. 7, it has not been possible to get a complete refinement from the neutron scattering data. Nevertheless, we can analyze the proposed space groups and compare the results of the group theory analysis with our data. Let us start with $Pmca$ which is a nonstandard setting of the $D_{2h}^{11}, Pbcm$ (No. 57). The unit cell contains 56 atoms, and in this case we cannot reduce the unit cell as was possible for the room temperature crystal structure. The expected number of modes is 168. Group theory predicts the following modes for this phase

$$23A_g + 18A_u + 24B_{1g} + 19B_{1u} + 16B_{2g} + 27B_{2u} + 15B_{3g} + 26B_{3u}$$

The A_u modes are silent. Thus, there are 78 Raman-active modes ($23A_g + 24B_{1g} + 16B_{2g} + 15B_{3g}$) and 72 infrared-active modes ($19B_{1u} + 27B_{2u} + 26B_{3u}$). It is clear from this analysis that one should expect a dramatic increase in the number of modes in the low temperature phase. Some of the new modes are the former Brillouin-zone-boundary modes which become visible because of the unit cell doubling; others are due to the lifting of degeneracy of former T and E-type modes. Some modes persist over the transition. For instance, the A_{1g} mode of the cubic phase becomes an A_g mode of the orthorhombic phase, having the same Raman tensor.

The second proposed symmetry is $C_{2v}^2, Pmc2_1$, (No. 26). This group does not contain an inversion center, leading to very important consequences for the Raman and infrared spectra. Namely, if magnetite has such a structure below $T_{\rm V}$, both infrared-active and Raman-active type modes should be detected by both spectroscopes. Experimentally, this is not the case and we can rule this symmetry out.

The symmetry of the Raman modes can be figured out by their polarization selection rules. The A_g and E_g-type modes have diagonal Raman tensor so that they are seen only when the polarizations of the incident and scattered light are parallel. In contrast, the T_{2g}, B_{1g}, B_{2g} and B_{3g} modes have off-diagonal components so that they are observed when the

polarizations of the incident and scattered light are perpendicular.

II. EXPERIMENTAL

The magnetite single crystals used in this work were grown by a chemical vapor transport technique using stoichiometric Fe_3O_4 microcrystalline powder obtained by reduction reaction of ferric oxide (Fe_2O_3). This procedure yielded near-stoichiometric crystals with typical size of 4x4x2 mm^3. X-ray diffraction confirmed the spinel-type structure of the crystals. Transport measurements found the abrupt increase in resistance below $T = 120$K, characteristic of the Verwey transition. Optical measurements were carried out on the optically smooth surfaces of the as-grown single crystals.

The reflectance was measured in the frequency range of 50–45000 cm^{-1} (6 meV–5.5 eV) at several temperatures between 40 and 300 K. The sample temperature was maintained by mounting the crystal on the cold-finger of a He-flow cryostat. To cover a wide frequency range, we used three optical set-ups. A Bruker IFS 113V spectrometer was employed for the far infrared and mid infrared regions (50–4500 cm^{-1}; 6–550 meV), a Perkin Elmer 16U grating spectrometer for the near infrared and visible region (3800–24000 cm^{-1}; 0.47–3 eV). We observed no temperature dependence of the spectra above 20000 cm^{-1}. Therefore, in order to extend the data to higher frequencies (20000-45000 cm^{-1}; 2.5–5.5 eV) we merged the spectrum at a given temperature with the room temperature reflectance spectrum obtained from a Zeiss grating spectrometer coupled with microscope, and finally in the frequency range above 45000 cm^{-1} we merged our data with the data of Ref. 16.

In order to analyze the optical properties of the sample we performed Kramers-Kronig transformation of reflectance data. For the temperatures above the transition, we use Drude-Lorentz model fit in the low frequency part of the spectrum. Then we calculated the reflectance and used the result for the low-frequency extrapolation. Below the transition, we assume constant DC conductivity at zero frequency as a low frequency approximation. For the high frequency approximation, we used a power law (ω^{-4}) extrapolation.

The polarized Raman scattering experiment was conducted a wide range of temperatures (T = 5–300 K) using a triple spectrometer equipped with a liquid-nitrogen cooled CCD detector. The 514.5 nm line of an Ar^+ laser was used as excitation with nominally 25 mW incident on the sample. The spectra were taken in the back-scattering geometry with the scattered light polarized vertically while the incident light is polarized to select a particular component of the Raman scattering tensor.

III. RESULTS AND DISCUSSION

A. Infrared and Raman-active Phonons

We now proceed to analyze the infrared and Raman data keeping in mind all of the above-predicted changes. The infrared reflectance and optical conductivity are shown in Fig. 1 and 2, while the Raman-scattering spectra of Fe_3O_4 are in Fig. 3. Oxygen phonon modes usually have their frequency above 200 cm^{-1}, whereas vibrations of the heavier iron atoms should be at much smaller frequency. In Fig. 1 and 2, two T_{1u} oxygen modes are found near 350 cm^{-1} and 560 cm^{-1}. These peaks are similar to the infrared-active phonons reported earlier by different groups.[17–20] Four Raman-active phonons are observed at room temperature in Fig. 3. The strongest peak at ≈670 cm^{-1} is either the A_{1g} or the E_g mode since it is only present in the parallel polarization geometry (XX). Since we expect the A_{1g} mode to have the highest frequency as it involves the stretching vibrations of the oxygen atoms along the Fe(A)-O bonds, the 670 cm^{-1} phonon is assigned to the A_{1g} mode. In Fig. 3, Raman spectrum in which the incident and scattered light polarizations are perpendicular contains the predicted three T_{2g} modes at 193 cm^{-1}, 308 cm^{-1}, and 540 cm^{-1}. Verble[21] made a similar assignment of the Raman-active phonons in Fe_3O_4 except for the 193 cm^{-1} which he did not observe. Instead, he reported that the lowest frequency T_{2g} mode is at 300 cm^{-1} as observed in the spectrum at T = 77 K. However, this feature seen by Verble at T = 77 K ($< T_V$) is related to the structural symmetry-breaking that occurs below T_V as discussed

below.

The Verwey transition manifests itself in both infrared and Raman spectra by remarkable changes in the phonon spectrum as the temperature is lowered through T_V. In the Raman spectrum, one can see at least 17 new modes below T_V. In addition to the new phonon modes there is a broad (about 150 cm^{-1}, full width on half maximum) peak with a maximum at 350 cm^{-1}. Unfortunately, with so many additional phonon modes it is difficult to judge whether this broad peak is a superposition of phonon modes or a background on which phonon modes are sitting.

There are several additional infrared modes as well. In Fig. 1 and 2b, in addition to the infrared active phonons near 350 cm^{-1} and 560 cm^{-1}, weak phonon features appear below 300 cm^{-1}. Similar effects are observed in the Raman spectrum at $T = 5$ K as illustrated in Fig. 3. Moreover, the Verwey transition also leads to renormalization of the phonon frequencies and linewidths. The infrared- and Raman-active phonons which persist over the transition were fitted to Lorentzian lineshapes in order to obtain their frequency and linewidths. The results of this analysis are shown in Fig. 4. For the infrared active phonons at 350 cm^{-1} and 560 cm^{-1}, the phonon frequencies increase upon decreasing the temperature but without visible anomalies around T_V. On the other hand, their linewidths manifest an abrupt increase near T_V. Additionally, for the 350 and 560 cm^{-1} phonons there is a reproducible fine structure in the reflectance; see Fig. 1b. At temperatures below the transition the lineshape of the 350 and 560 cm^{-1} phonons can not be described by a single Lorentzian, which leads to bigger error bars for the linewidth and frequency of these phonons below the transition. See Fig. 4. Note that in contrast to the Chakraverty[13] result, within our experimental error we do not observe any soft optical mode.

The observed phonon anomalies can be explained in the following way. Above the transition most of the phonon modes are highly degenerate modes. When magnetite undergoes the Verwey transition, the crystal symmetry reduces to orthorhombic, lifting the degeneracy of the modes. We suggest that splitting, determined by the degree of distortion associated with the symmetry changes, will not be too large. According to the neutron data[7] the Fe-O

distances for both A and B sites are generally within the estimated standard deviations for the prototype structure; therefore, one expects the splitting to be small, appearing as a broadening of the modes above the transition. This is what has been observed in our experiment for the two infrared active modes at 350 and 560 cm^{-1}.

The frequency and linewidth of the Raman-active phonon at 670 cm^{-1} in Fig. 4 shows an abrupt increase in frequency with a concomitant precipitous drop in the linewidth at T_V. The symmetry of this mode in the cubic phase is A_{1g}; it corresponds to the in-phase vibrations of the oxygen ions forming tetrahedra surrounding the Fe ions in the A positions.[21] At the same time, a similar type of displacement for the cubic-orthorhombic structural transition has been found from neutron measurements.[7] Therefore, it is plausible to assume that 670 cm^{-1} phonon is directly coupled to the structural displacements at the Verwey transition. This is the reason why this mode is so sensitive to the transition.

B. Charge Dynamics

At room temperature, in addition to the phonon features, one notes a gradual decline of reflectance (Fig. 1a) towards higher frequencies with a distinctive minimum at about 10000 cm^{-1} and some weak and almost temperature independent transitions occurring in the visible and ultra violet region.

With decreasing temperature, the low frequency reflectance (below 1000 cm^{-1}) decreases. Below T_V a minimum forms at $\approx$ 750 cm^{-1}, followed by increased reflectance, with a temperature- dependant hump around 4000 cm^{-1}. Above 20000 cm^{-1}, the reflectance is practically temperature independent.

The optical conductivity derived from the reflectance data is shown in Fig. 2. Aside from the phonon peaks, one notes a decrease of the low frequency conductivity (below 1000 cm^{-1}) with decreased temperature as well as a broad temperature-dependent band at 5000 cm^{-1}. The intensity of this band increases with decreased temperature followed by slight temperature dependent increase of the conductivity towards higher frequencies. The

most interesting aspect of the data is the temperature-dependence, which we will discuss next.

We will base our discussion on the local density approximation calculations of Ref. 22. According to these calculations of the single-electron density of states, there are O($2p$) bands lying about 4 eV below Fermi level which is found in the middle of the Fe($3d$) bands. Therefore, the interesting physics relevant to the Verwey transition is connected with these Fe($3d$) bands. Within the Fe($3d$) bands one should pay special attention to the two spin-polarized bands. Let us recall that there are two magnetic sublattices corresponding to the A and B positions in the unit cell, with the spins parallel to each other within one sublattice and antiparallel to the spins in another sublattice. From the electronic structure,[22] one expects a peak in the optical conductivity associated with the optical transition from B site to B site. It is clear that such a peak should be sensitive to the Verwey transition because the B sites are the sites where ordering takes place. A good candidate for this peak is the 5000 cm^{-1} peak, which changes in intensity with temperature. In the framework of the Mott model[10] of the Verwey transition this is the polaronic peak. The increase in oscillator strength above 10000 cm^{-1} is attributed to the oxygen-iron optical transitions, although some optically allowed transitions from A to B site may also contribute.

Another striking feature which should be explained is a gap-like feature in the optical conductivity at 1000 cm^{-1} at temperatures below the Verwey transition. To analyze changes of conductivity we estimate the oscillator strength or spectral weight in the low-energy region. The effective number of carriers (per Fe^{+2} ion) participating in optical transitions at frequency less than ω is defined as[23]

$$\frac{m}{m^*}N_{eff}(\omega) = \frac{2mV_{cell}}{\pi e^2 N_{\mathrm{Fe}^{+2}}}\int_0^{\omega}\sigma_1(\omega')d\omega',$$

where m is the free-electron mass, m^* is the effective mass of the carriers, V_{cell} is the unit-cell volume, and $N_{\mathrm{Fe}^{+2}}$ is the number of Fe^{+2} ions per unit cell.

One can clearly see in Fig.5 an increase of N_{eff} with temperature. For temperatures below the transition, we found the maximum change in this quantity at frequencies around

1800 cm^{-1}. In order to compare the temperature dependence of N_{eff} with the DC conductivity, we show the N_{eff}(1800 cm^{-1}), for different temperatures together with the conductivity in the insert of Fig.5. The sharp increase of N_{eff} closely resembles the very similar increase in conductivity at the Verwey transition. A similar result was shown by Park et al.[15]

One should note that there are several ways to interpret the gap-like feature in the conductivity. One can assign such a behavior either to an activated mobility of the form $\mu_0 \exp(-W_H/k_B\mathrm{T})$, where W_H is the polaron hopping energy, or to the opening of a charge gap Δ. In later case the carrier concentration will behave like $n_0 \exp(-\Delta/k_B\mathrm{T})$, leading to activated conductivity as well. It is clear that both effects may alter the conductivity. However, the agreement of N_{eff} and the conductivity suggests activation of the free carrier density.

Using the definition of N_{eff} we can try to estimate effective mass of the carriers. Let us assume that N_{eff}(1800 cm^{-1}) is purely due to the free carrier optical conductivity. In this case, using the definition of N_{eff}, we can expect N_{eff}(1800 cm^{-1}, 300K)$\approx m/m^*$, which gives us $m^* \approx 100m$. Now let us compare this number to the effective mass from Mott equation:[10]

$$m^* \approx 5m \exp(W_H/\frac{1}{2}\hbar\omega),$$

where $\hbar\omega$ is the zero-point phonon energy.

We can get the value of W_H from the polaron peak position. Namely, the peak position ($\approx$ 5000 cm^{-1}) gives us $2W_B$, where W_B is the polaron binding energy. In the simple model of an electron jumping between two molecules[12] the hopping energy can be estimated as $W_H \approx 1/2W_B$, yielding $W_H = 1250$ cm^{-1}. The zero-point phonon energy can be estimated to be the frequency of the highest-energy optical phonon, 670 cm^{-1}. These estimates give $m^* \approx 200m$, the same order of magnitude that we estimated from N_{eff}. Note that the Mott formula contains an exponent which is very sensitive to both value of W_H and $\frac{1}{2}\hbar\omega$, therefore the fact that we have got the right order of magnitude for the effective mass is consistent with the idea of a polaron mechanism of conductivity in magnetite.

IV. CONCLUSIONS

We have presented results for infrared and Raman measurements of magnetite. Both Raman and infrared spectroscopic techniques observed phonon anomalies at T_V which are attributed to the symmetry and structural changes below T_V. We are able to rule out a structure lacking inversion symmetry.

Our optical data seem to fit to the following description. At the temperatures below T_V carriers are localized polarons and we have a strong polaron peak at ≈ 5000 cm^{-1} and a gaplike decrease of optical conductivity below 1000 cm^{-1}. All polarons are bound and position of the polaron peak occurs at twice the binding energy.

At temperatures above the transition, some carriers are delocalized, leading to removal of oscillator strength from the 5000 cm^{-1} peak, broadening, and an increase of the low-frequency conductivity. It is difficult to separate effects of the filling of the charge gap or the activated increase of mobility. However, no matter what is causing it, the low frequency optical conductivity follows the DC conductivity. The increase of the 5000 cm^{-1} band oscillator strength with decrease of the temperature is consistent with the polaronic origin of this band, consistent with the previous observations of Park et al.[15] The effective mass of the carriers estimated from the optical conductivity gives a value of $\approx 100m$, close to that predicted by Mott in the framework of the polaron model of the Verwey transition. All these observations strongly indicate the importance of lattice dynamics effects, favoring the polaronic picture of the Verwey transition.

ACKNOWLEDGMENTS

Work at Florida was supported by NSF grant DMR-9705108. L.V.G acknowledges Dr. E. Ya. Sherman for the critical discussion of the manuscript. D.B.R. acknowledges Dr.Raju Datla for his interest in and support of the Raman work at NIST. H.B. wishes to express appreciation to Dr. J. Lammer for fruitful discussions.

REFERENCES

[1] J.D. Axe *et al.*, Phys. Rev. Lett. **62,** 2751 (1989).

[2] J.M. Tranquada *et al.*, Phys. Rev. Lett. **78,** 338 (1997).

[3] M. Fischer, P. Lemmens, G. Els, G. Güntherodt, E. Sherman, E. Morre, C. Geibel, and F. Steglich, submitted to Phys. Rev. B

[4] S. Mori, C.H. Chen, and S.-W. Cheong, Nature **392,** 473 (1998).

[5] E.J.W. Verwey, Nature **144**, 327 (1939).

[6] W.H. Bragg, Phil. Mag.**30**, 305 (1915).

[7] M. Iizumi, T.F. Koetzle, G. Shirane, S. Chikazumi, M. Matsui, S. Todo, Acta Cryst. B**39**, 2121 (1982).

[8] E.J.W. Vervey and P.W. Haayman, Physica, **8**, 979 (1941).

[9] P.W. Anderson, Phys. Rev. **102**, 1008 (1956).

[10] N.F. Mott, Phil. Mag. **42**, 327 (1980).

[11] J.R. Cullen, E.R. Callen, J.Appl. Phys. **41**, 879 (1970).

[12] I.G. Austin, N.F. Mott, Adv. Phys. **18**, 41 (1969).

[13] B.K. Chakraverty, Solid State Commun. **15**, 1271 (1974).

[14] Y. Yamada, Phil. Mag. **42**, 377 (1980).

[15] J.-H. Park, L.H. Tjeng, J.W. Allen, P. Metcalf, C.T. Chen, Phys. Rev. B**55**, 12813 (1997).

[16] S.K. Park, T. Ishikawa, Y. Tokura, Phys. Rev. B **58**, 3717 (1998).

[17] A. Shlegel, S.F. Alvarado, P. Wachter, J. Phys. C, **12**, 1157 (1979).

[18] A. Shlegel, P. Wachter, J. de Phys. **C5**, 19 (1980).

[19] L. Degiorgi, I. Blatter-Mörke, P. Wachter, Phys. Rev. B **35** 5421.

[20] L. Degiorgi, P. Wachter, D. Ihle, Phys. Rev. B **35** 9259.

[21] J.L. Verble, Phys. Rev B **9**, 5236 (1974).

[22] Z. Zgang and S. Satpathy, Phys. Rev. B **44**, 13319 (1991).

[23] F. Wooten, in *Optical Properties of Solids* (Academic Press, New York, 1972).

FIGURES

FIG. 1. a) The reflectance of magnetite in the frequency range from 50 to 45000 cm^{-1} b) The low-frequency (up to 700 cm^{-1}) reflectance of magnetite at temperatures above and below the Verwey transition.

FIG. 2. The optical conductivity of magnetite calculated by the Kramers-Kronig transformation of the reflectance data. Fig. 2a shows the optical conductivity below 45000 cm^{-1} and Fig. 2b shows the low frequency optical conductivity (up to 700 cm^{-1}) at temperatures above and below the Verwey transition.

FIG. 3. The Raman spectrum of magnetite at temperatures above and below the Verwey transition. Shown are spectra in the XX-geometry and XY-geometry. The insert shows the XX-spectrum below 600cm^{-1}.

FIG. 4. The frequency (solid circles) and linewidth (opened circles) of the infrared and Raman modes as determined by Lorentzian fits to the data.

FIG. 5. The effective number of carriers participating in optical transitions at frequencies below ω ($N_{eff}(\omega)$) versus ω at temperatures above and below the Verwey transition. The insert shows N_{eff} at 1800 cm^{-1} versus temperature (solid circles), and the DC conductivity versus temperature (open circles).

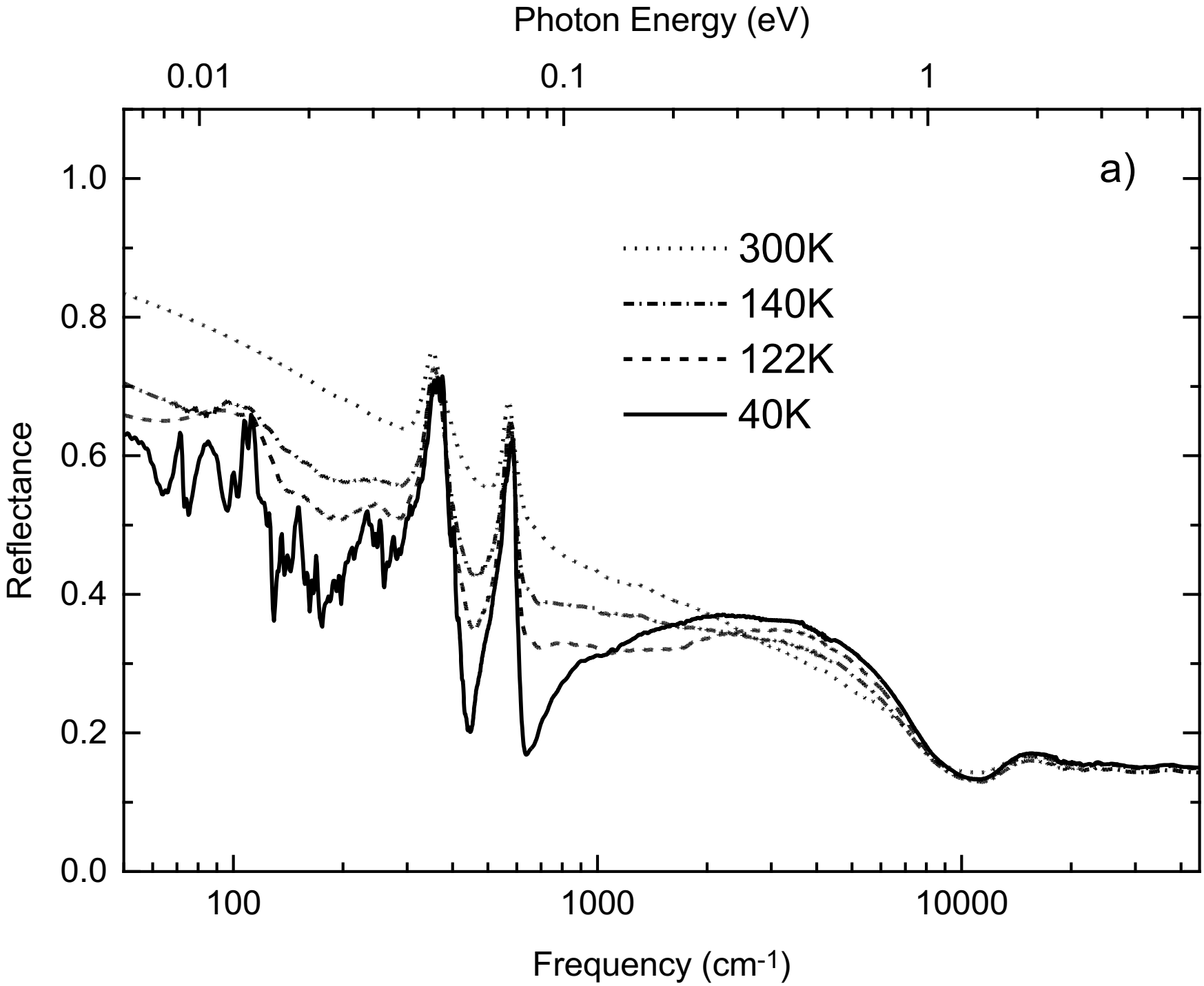
Photon Energy (eV)
0.01
0.1
1
a)
300K
140K
122K
40K
Reflectance
1.0
0.8
0.6
0.4
0.2
0.0
100
1000
10000
Frequency (cm-1)

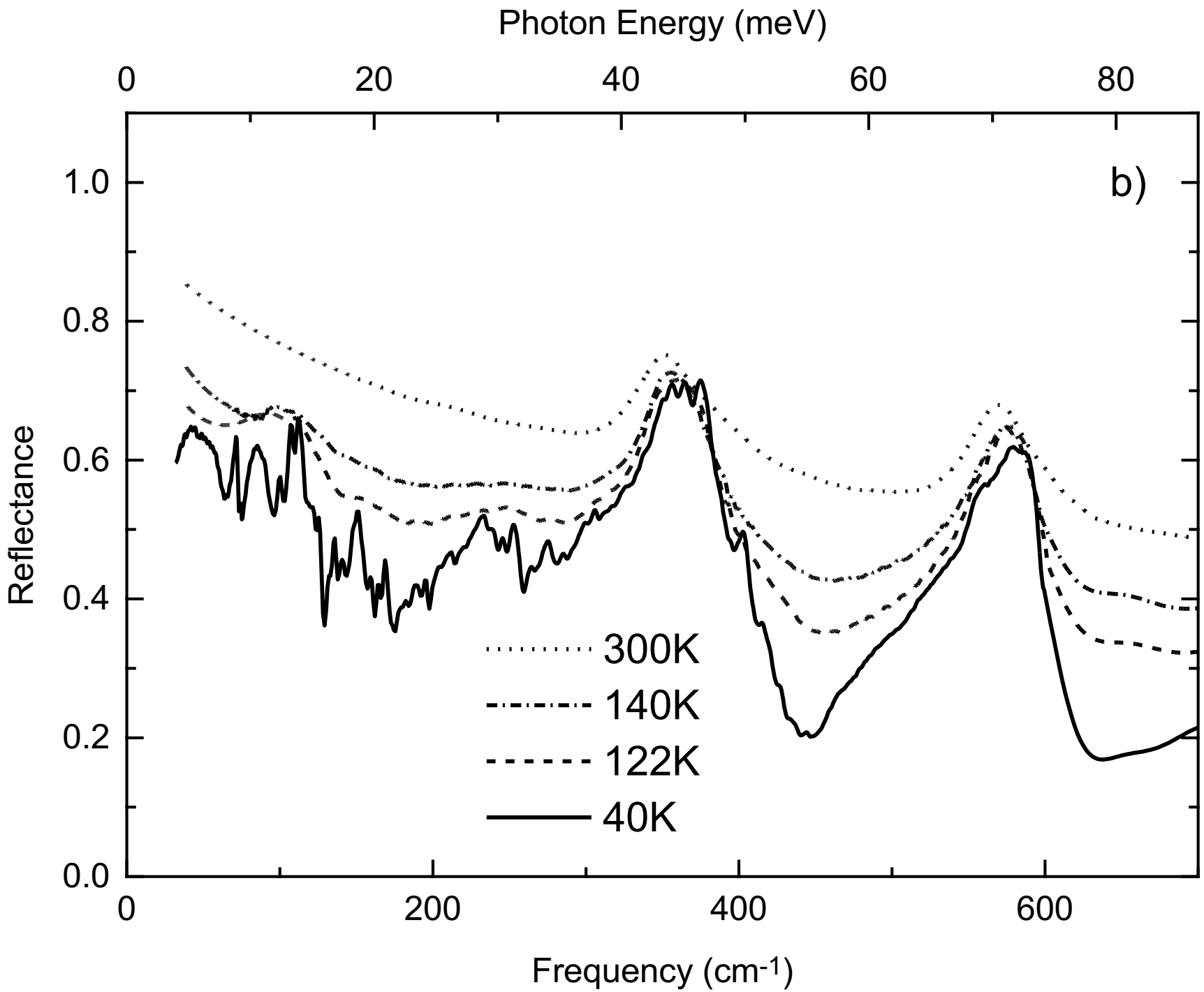
Photon Energy (meV)
0
20
40
60
80
b)
1.0
0.8
0.6
0.4
0.2
0.0
Reflectance
300K
140K
122K
40K
0
200
400
600
Frequency (cm-1)

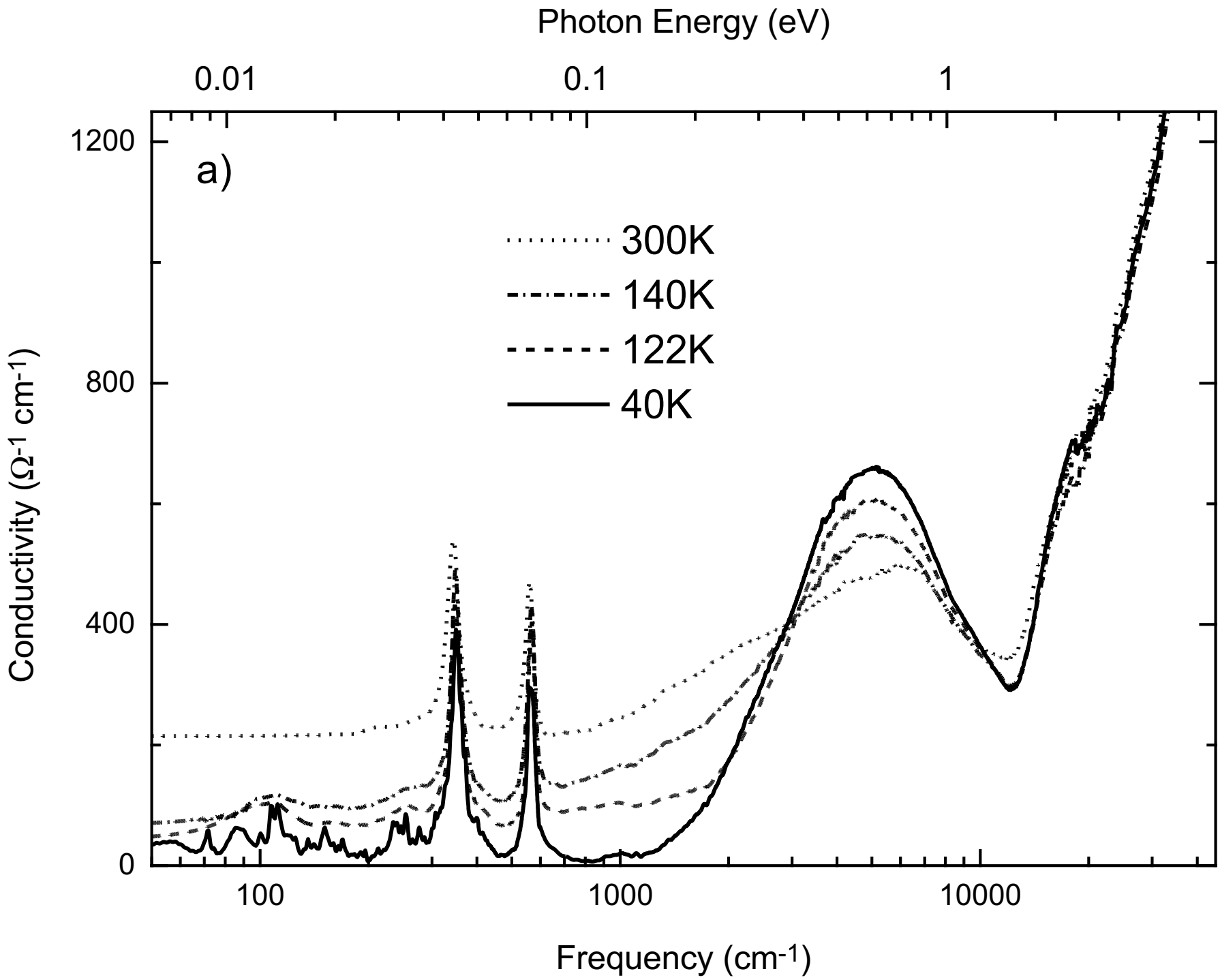
Photon Energy (eV)
0.01
0.1
1
a)
300K
140K
122K
40K
Conductivity (Ω-1 cm-1)
1200
800
400
0
100
1000
10000
Frequency (cm-1)

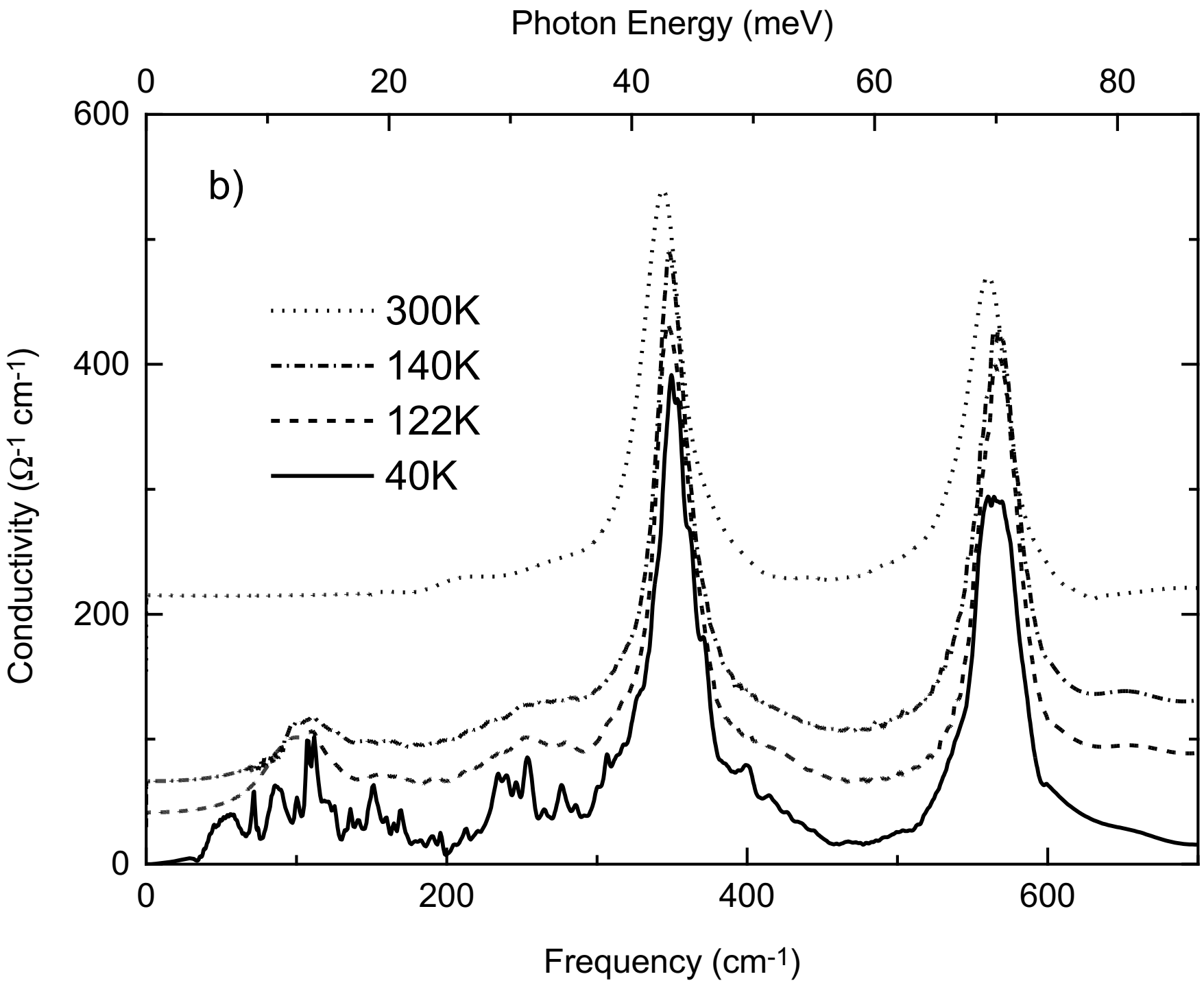
Photon Energy (meV)
0
20
40
60
80
600
400
200
0
b)
300K
140K
122K
40K
Conductivity (Ω-1 cm-1)
0
200
400
600
Frequency (cm-1)

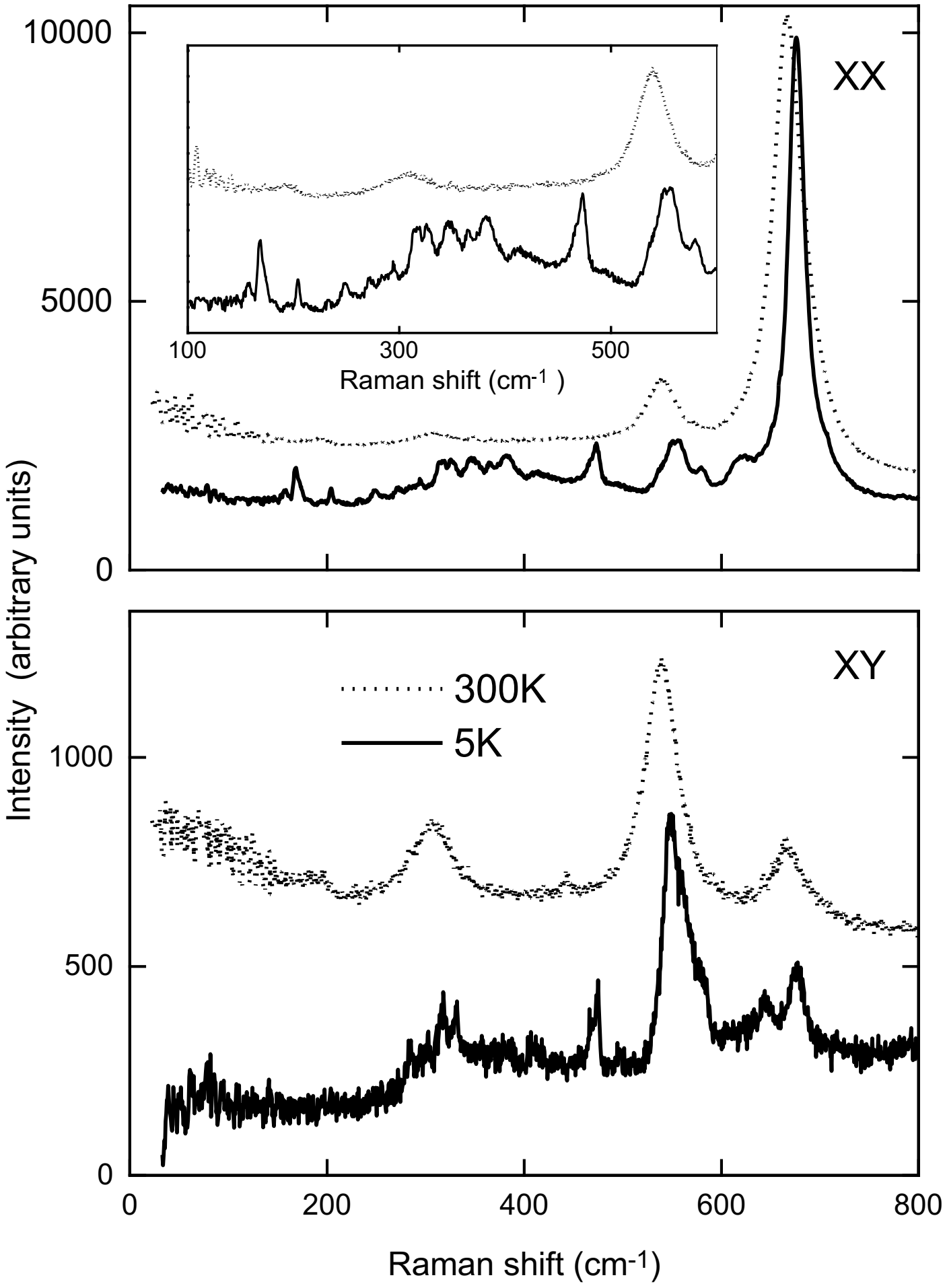
10000
5000
0
XX
100
300
500
Raman shift (cm-1)
Intensity (arbitrary units)
1000
500
0
XY
300K
5K
0
200
400
600
800
Raman shift (cm-1)

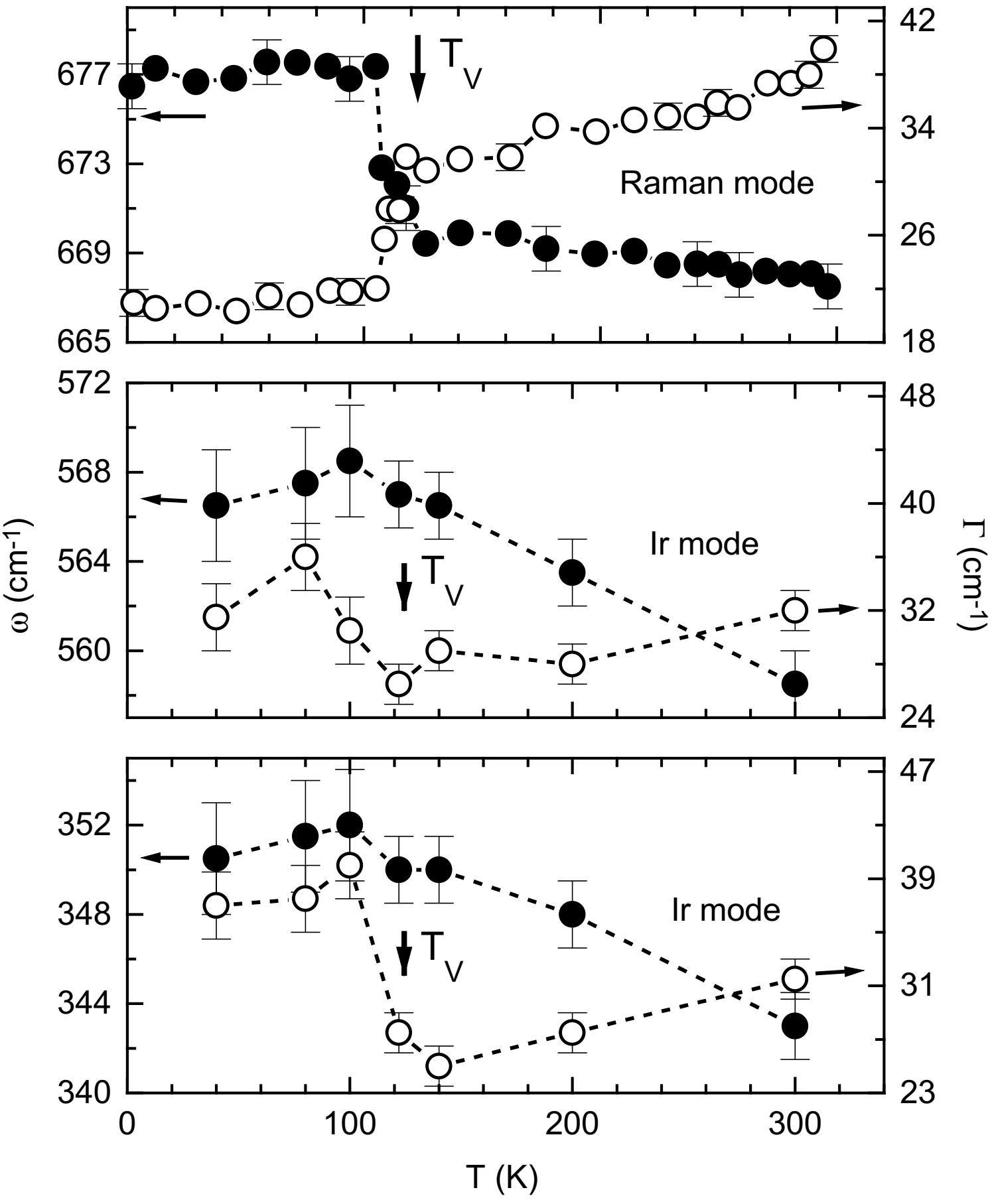
677
673
669
665
42
34
26
18
T_V
Raman mode
572
568
564
560
48
40
32
24
Ir mode
T_V
ω (cm^{-1})
Γ (cm^{-1})
352
348
344
340
47
39
31
23
Ir mode
T_V
0
100
200
300
T (K)

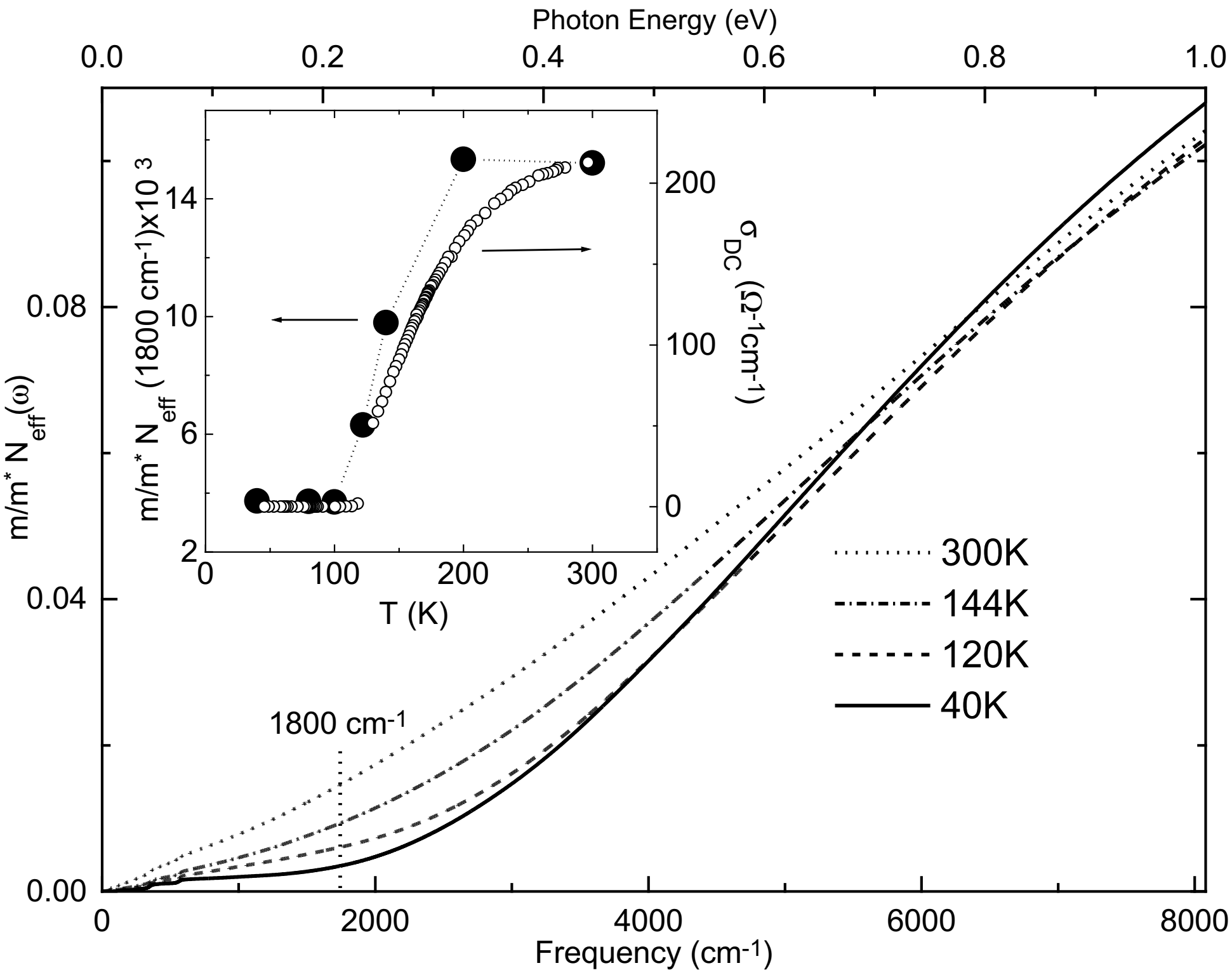
Photon Energy (eV)
0.0
0.2
0.4
0.6
0.8
1.0
m/m* N_eff(ω)
0.00
0.04
0.08
0
2000
4000
6000
8000
Frequency (cm-1)
1800 cm-1
300K
144K
120K
40K
m/m* N_eff (1800 cm-1)x10 3
2
6
10
14
T (K)
0
100
200
300
σ_DC (Ω-1cm-1)
0
100
200